

Article

The Influence of Microstructured Charcoal Additive on ANFO's Properties

Andrzej Biessikirski ^{1,*}, Suzana Gotovac Atlagić ^{2,*}, Mateusz Pytlik ³, Łukasz Kuterasiński ⁴,
Michał Dworzak ¹, Michał Twardosz ¹, Dagmara Nowak-Senderowska ¹ and Bogna Daria Napruszewska ⁴

¹ Faculty of Civil Engineering and Resource Management, AGH University of Science and Technology, Al. Mickiewicza 30, 30-059 Kraków, Poland; dworzak@agh.edu.pl (M.D.); michaltw@agh.edu.pl (M.T.); nowaksen@agh.edu.pl (D.N.-S.)

² Faculty of Natural Sciences and Mathematics, University of Banja Luka, Mladena Stojanovića 2, 78000 Banja Luka, Bosnia and Herzegovina

³ Conformity Assessment Body, Central Mining Institute, Plac Gwarków 1, 40-166 Katowice, Poland; mpytlik@gig.eu

⁴ Jerzy Haber Institute of Catalysis and Surface Chemistry, Polish Academy of Sciences, ul. Niezapominajek 8, 30-239 Kraków, Poland; lukasz.kuterasiński@ikifp.edu.pl (Ł.K.); bogna.napruszewska@ikifp.edu.pl (B.D.N.)

* Correspondence: abiess@agh.edu.pl (A.B.); suzana.gotovac.atlagic@unibl.org (S.G.A.); Tel.: +48-12-67-20-70 (A.B.)

Abstract: The verification of the blasting parameters of Ammonium Nitrate Fuel Oil (ANFO) with the addition of microstructured charcoal (MC) produced by destructive wood distillation was performed. Additional investigation of specific surface and pore distribution by the nitrogen adsorption of the two granulations of MC was also carried out. High-resolution scanning electron microscopy was used for morphology evaluation and revealed smoothening of the initially developed external surface of carbon with intensive milling. In addition, the analysis of the thermal properties of the studied samples (TG/DSC) indicated that the size of the microstructured charcoal additives influenced the decomposition temperature of the prepared materials. The explosives containing microstructured charcoal grains of $-90\ \mu\text{m}$ underwent decomposition at lower temperatures in comparison with those containing higher sizes of microstructure charcoal grains ($-1.18\ \text{mm}$), for which the decomposition temperature reached $292\ ^\circ\text{C}$. The obtained results of blasting parameters compared to the results derived from thermodynamic simulation showed the non-ideal character of the explosives (much lower values of blasting parameters than in established thermodynamic models). It was indicated that higher velocities of detonations (VOD) were obtained for non-ideal explosives where finer MC grains were added. Blasting tests confirmed that the studied type of MC can be applied as an additive to the ANFO.

Keywords: ANFO; microstructure charcoal; explosives; blasting properties



Citation: Biessikirski, A.; Gotovac Atlagić, S.; Pytlik, M.; Kuterasiński, Ł.; Dworzak, M.; Twardosz, M.; Nowak-Senderowska, D.; Napruszewska, B.D. The Influence of Microstructured Charcoal Additive on ANFO's Properties. *Energies* **2021**, *14*, 4354. <https://doi.org/10.3390/en14144354>

Academic Editor: M. Toufiq Reza

Received: 23 June 2021

Accepted: 15 July 2021

Published: 19 July 2021

Publisher's Note: MDPI stays neutral with regard to jurisdictional claims in published maps and institutional affiliations.



Copyright: © 2021 by the authors. Licensee MDPI, Basel, Switzerland. This article is an open access article distributed under the terms and conditions of the Creative Commons Attribution (CC BY) license (<https://creativecommons.org/licenses/by/4.0/>).

1. Introduction

Ammonium nitrate fuel oil (ANFO) is a mixture of ammonium nitrate (V) (AN) with a fuel oil (FO) with a weight ratio which should ensure zero oxygen balance. Usually, the weight ratio between AN and FO is 94.5:5.5, however, due to the possible modification in FO composition or the application of a different type of fuel oil, the weight ratio between oxygen and the fuel component can change slightly. In addition, it should be noted that various types of the oxygen component can be used. Usually, ammonium nitrate (V) porous prill (AN-PP) is used as the oxygen component and this is recommended by a number of pieces of research [1–3]. However, in some cases (usually in Improvised Explosive Devices), the fertilizer grade of ammonium nitrate (V) (AN-F) is used. The main difference between AN-F and AN-PP is the lower density, higher retention, and higher absorption index (AN-PP is ca. 12–16% and AN-F ca. 8%) of AN-PP which can be explained by higher porosity and the presence of numerous surface deformations in AN-PP prills [1–4].

Furthermore, Landucci et al. indicated that AN which is used in mining explosives has a 20% void fraction and is much more energy-efficient [5].

At present, ANFO is one of the most popular explosives which is applied in the mining industry around the world, mainly due to its low cost of manufacturing, the simplicity of its production, and the vast possibilities of designing blasting properties (not only by adjusting FO or AN-PP content but also by applying other metals or inert components) [6,7]. However, the non-ideal character of ANFO should be highlighted. Miyake et al. stated that non-ideal behavior can be observed based on the velocity, which does not reach its theoretically predicated values. They also indicated that AN based explosives behave non-ideally between a critical diameter (relatively small values), below which a steady detonation wave cannot be sustained [8]. Zygmunt and Buczkowski highlighted that the detonation process of ANFO is a typical non-ideal detonation model which may be influenced by the physiochemical parameters of ammonium nitrate (V). Moreover, they indicated that the change of the physiochemical parameters may affect ANFO's detonation parameters to a high degree [7]. Moreover, the application of additives or inert component to the non-ideal composition influences the reaction zone (in some cases it extends the chemical reaction zone when metals like aluminum are added) which results in the shift of the Chapman-Jouguet plain. Furthermore, with the application of a new component, the oxygen balance changes which, due to their influence on blasting properties, should be taken into consideration.

The possible application of coal powders was discussed in research [9–13]. Miyake et al. investigated, through steel tube tests, the detonation characteristics, as well as the velocity of detonation (VOD) of various forms of AN with activated carbon (AC) mixtures [9,11,12]. They concluded that powdered AN:AC compositions have higher detonation velocities than phase-stabilized AN mixtures. Moreover, VOD raised with an increased content of AC (with 5% AC content VOD reached $3400 \text{ m}\cdot\text{s}^{-1}$) [9]. In further tests, it was established that depending on the charge diameter, the VOD was in the range $2950\text{--}3700 \text{ m}\cdot\text{s}^{-1}$ and pressure peak in the range of $1.95\text{--}4.90 \text{ GPa}$ [11,12]. The obtained results were far below those predicated by CHEETAH codes and the BKWC equation of state. They showed that VOD increases in a linear manner with an energy release at the detonation front, which should be in contrast to the detonation pressure. It was assumed that detonation pressure increases in other functions, like the square of energy release [11,12]. Kubota et al. confirmed the non-ideal behavior of pure AN [13]. Moreover, they constructed and established size-effective curves of AN:AC mixtures [13]. Nakamura et al. performed friction tests on ammonium nitrate with carbon powder mixtures [10]. They established that the explosive samples were insensitive to friction. Additionally, the closed-vessel combustion test revealed that a 4% addition of carbon powder to AN resulted in a sudden exothermic reaction which begun after the AN had melted. The detailed thermal decomposition of AN and carbon mixtures was presented in papers [14,15]. Luri and Lianshen investigated the thermal decomposition of ammonium powder under the action of carbon black. They indicated that the presence of carbon black increases the decomposition rate of solid AN, which is proportional to the amount of carbon black powder. Furthermore, at a relatively low temperature, the decomposition process is proceeded by a two-stage mechanism with an acceleration mechanism at each stage. Izato et al. concluded that the crystallinity of carbon influences the thermal decomposition of AN: carbon mixtures, and also that these AN: carbon mixtures are oxidized by NO_x, which is formed from the decomposition of AN [15]. The content of CO and NO_x is a crucial factor which should be taken into consideration when concerning potential MC addition to ANFO. Bhattacharyya et al. showed that detonation of finer-grained ANFO resulted in a higher concentration of NO_x in post-blast oxides in comparison with the coarser-grained ANFO. They suggested that finer-grained ANFO reacts much faster in comparison with coarser-grained ANFO. One effect of this is that the more rapid the reaction is, the higher the volume of oxygen is available to the chemical reaction, which could lead to the formation of NO_x. However, Onederra et al. highlighted that these assumptions have

been refuted by a number of pieces of research like De Souza and Katsabanis, Sapko et al., and Mainiero et al. [16–19]. Sapko et al. indicated that the addition of pulverized ANFO generates four times less NO_x than regular ANFO [17]. This was explained by the better mix between fuel and AN (nitrate of pulverized AN prill), which led to a more complete decomposition reaction, as well as higher VOD. A number of in-situ tests have shown that the application of a product with less FO results in an increase of NO_x in post-blast fumes, while an excess of FO generates less NO_x. This is justified by a better stoichiometric mix of AN and FO [18–21]. Moreover, in the case of fuel lean product, an increased content of NO_x should be explained by the deflagration reaction. In such a reaction, carbon atoms from the FO are not available for the chemical reactions, which causes the nitrogen atoms from the AN to behave like a nitrogen-based fuel source. This leads to an increased volume of NO_x [19].

Despite access to numerous papers and technical reports in subject of ANFO, the possible application of MC and its influence on blasting properties was studied in a limited manner. The aim of this work was to make an evaluation of the following blasting parameters: heat of explosion, VOD, and the post-blast oxides of non-ideal explosives based on two different assortments of MC powders. This approach will enable the validation of experimental data presented in this paper [22]. Based on the HRSEM analysis presented in [22], it is expected that MC additives will have an influence on the volume of NO_x due to their complicated microstructure.

2. Materials and Methods

2.1. Materials

Ammonium nitrate porous prill (AN-PP) was mass-produced by Yara's International A SA; AN-PP which was synthesized in 2020 was distinguished by a bulk density of 0.82 g·cm⁻³ at 20 °C. Prill average size was 1 mm. The detailed morphological characteristics were provided in papers [4,22].

Microstructured charcoal (MC) in the form of powder was manufactured by the HI Destilacija Teslić in Bosnia and Herzegovina, and it was produced by the destructive wood distillation process. MC powders were characterized by a grain size of ~90 μm (fine powder) and ~1.18 mm (small granules). These two classes were chosen as representatives of utterly different morphologies where significantly different levels of mechanical forces were used to prepare the samples.

The fuel oil (FO), which is ANFO's flammable component, was produced by the Silesia Oil sp. z o.o. T Density of the FO was 800 kg·cm⁻³ and kinetic viscosity of FO was 13.6 mm²·s⁻¹. The detailed FO characteristics were provided in [4]. The fuel oil sample was manufactured in 2020.

The ANFO was produced in laboratory conditions by adding FO to the AN-PP at 250 rpm. The blending procedure lasted for 20 min. In order to obtain the non-ideal explosive with MC content, the MC sample was added to the ANFO for the last 5 min of the blending process.

All sample compositions are shown in Table 1.

Table 1. Non-ideal explosive compositions, % wt.

Sample Name	AN-PP, % wt.	FO, % wt.	MC, % wt.
Sample 1	94.5	5.5	-
Sample 2	94.5	4.5	1.0
Sample 3	94.5	2.5	3.0
Sample 4	91.0	6.0	3.0

2.2. Methods

A high-resolution scanning electron microscope (HR-SEM) was used with a voltage of 5.00 kV and a current of 0.1 nA. T2 and ETD detectors were used. The highest magnification at which clear images were obtained was 150,000×. The material was characterized by

the x-ray photoelectron spectroscopy (instrument “PHOIBOS”, with software “SpecsLab Prodigy”, model “4.34.1-r66167”). Lens analyzer: MediumArea: 1.5 kV, analyzer slit: $5:7 \times 20$ /B: open. Scanning program: FixedAnalyzerTransmission, retention time: 0.1, excitation energy 1486.61, binding energy 1400, pass energy 40, detector voltage: 2170. Specific surface and the pore-size distribution was measured by the Brunauer-Emmett-Teller (BET) method with 3P INSTRUMENTS Surface Area and Pore Size Analyzer, Sync 110A model. Samples were degassed at 200 °C for 2 h. The nitrogen was used as an adsorbate. Thermal analyses (Thermogravimetry—TG and Differential Scanning Calorimetry—DSC) of the AN prill were performed at 20–800 °C. All investigated materials were exposed to an airflow of 30 mL·min^{−1}. Instead of inert gases like nitrogen, an airflow was selected due to the fact it could sustain the similar conditions in the both the furnace and balance chamber like in the case of the typical explosive detonation. Directly prior to each measurement, the explosive sample (20 mg) was placed in the DSC aluminum pan using a spatula. The TG baseline was determined using a heating profile for the empty pan. The TG drift was ca. 5 µg, which constituted 0.02 mass%.

Thermodynamic calculations were made in the ZMWCyw software. The software was developed by the Military University of Technology in Warsaw. Calculations rely on the physico-chemical properties of each component. If component is not present in the ZMWCyw database, it can be defined and added by the user. ZMWCyw software allows for the calculation of parameters like the explosion pressure and temperature heat of the explosion, the post-blast volume, etc. The oxygen balance of each individual explosive material was calculated according to the standard [23].

Measurements of the heat of explosives were performed in a detonation calorimeter. The 50 g non-ideal explosive sample was initiated with an Erg electric detonator and a 5 g RDX booster. The obtained results took into account the characteristic temperatures of the cycles (T_1 – T_4), the duration of the main period of the cycle (n), and the total heat effect (Q) calculated for the preset heat capacity of the assembly (K), which were read after completing the measurement. The total heat effect was calculated using (1).

$$Q = K \times (\Delta T - k) \quad (1)$$

where K indicates the heat capacity of the assembly, cal °C; ΔT —the differentiation of the temperature during the main period of the cycle; $\Delta T = T_3 - T_2$, °C; T_1, T_2, T_3, T_4 —the distinguished temperatures in characteristic points of the measurement cycles, °C; k —the coefficient which is responsible for making a correction on losses of the assembly, °C, computed based on Equation (2):

$$k = 0.5 \times [0.2 \times (T_2 - T_1) + 0.2 \times (T_4 - T_3)] + 0.2 \times (n - 1) \times (T_4 - T_3) \quad (2)$$

where n denotes the duration of the main period of the cycle, min.

A detailed description of measurements of the heat of the explosion is provided in [24].

Post-blast oxide analysis was performed according to the standard [25], which is in accordance with the council directive [26]. Non-ideal explosive charges of a mass of 600 g were placed inside the steel mortar which was inside the blasting chamber (Figure 1). After the blasting chamber was sealed, explosive charges were detonated.

After decomposition reaction, the fan system was activated in order to achieve the homogenization of the post-blast fumes. The homogenization process lasted 3 min. Subsequently, post-blast gases samples were collected for 20 min in the ventilation system. The amounts of CO and CO₂ were determined by IR (MIR 25e) and NO_x by chemiluminescent (TOPAZE 32M) analyzers.

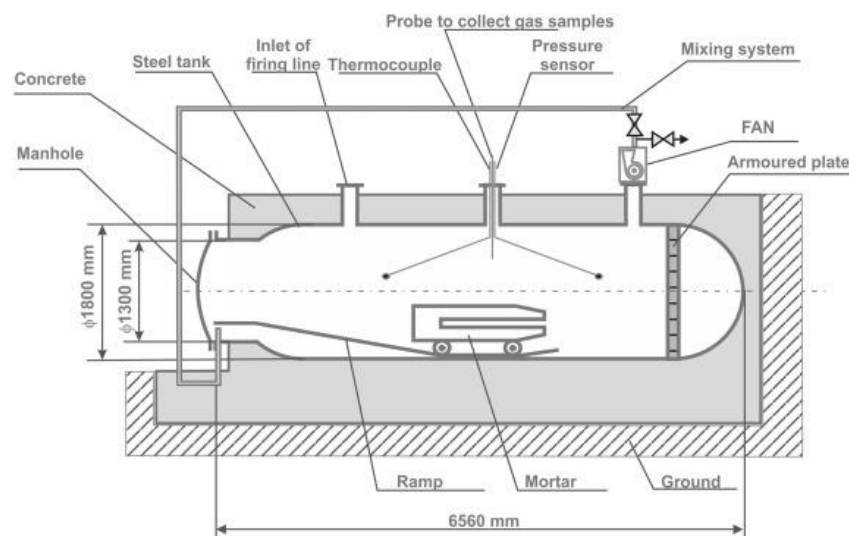


Figure 1. Blasting chamber [27].

The velocity of detonation (VOD) was measured based on the standard [28] by blasting 600 g of non-ideal explosive charge in a glass pipe. The pipe's inner diameter was 46 mm. VOD was measured by placing two short-circuit probes close to the top and bottom of the tube. The distance between the probes was 150 mm. The VOD was established by the division of the time difference which was derived by the progressing detonation with a distance between probes (Equation (3)):

$$\text{VOD} = \frac{l}{t} \quad (3)$$

where l denotes the distance between two probes and t is the time difference [29].

All non-ideal explosives were initiated by the 14 g RDX (Royal Demolition Explosive)-based charge.

2.3. Microstructured Charcoal Characteristics

Figure 2 shows the comparative images of the two classes of carbon materials which were used in this research. The preliminary comment which can be made is that the carbon of $-90 \mu\text{m}$ class had a visibly smoother surface, while the carbon of -1.18 mm class had highly developed surface morphology with many uneven features over the surface. It can even be clearly concluded from the image taken at $100,000\times$ magnification that a number of pores and rainures below 100 nm were present. The smoother surface of the $-90 \mu\text{m}$ class sample can be explained by the mechanochemical reactions which probably took place during the intensive ball milling of the sample when the graphene layers overlapped, forming an apparent multilayered smooth-carbon structure with very few pores or irregularities visible. In the case of the -1.18 mm carbon, much less force was used since carbon was crushed to a granular size with a small mechanochemical action. Therefore, original structures which evolved in the process of the destructive wood distillation were more present. Since the process is very similar to the pyrolysis used in the activated carbon production, many pores and irregularities such as rainures formed on the surface with the process of the evaporation of liquid contents from the wood and under pressure of evolving vapors.

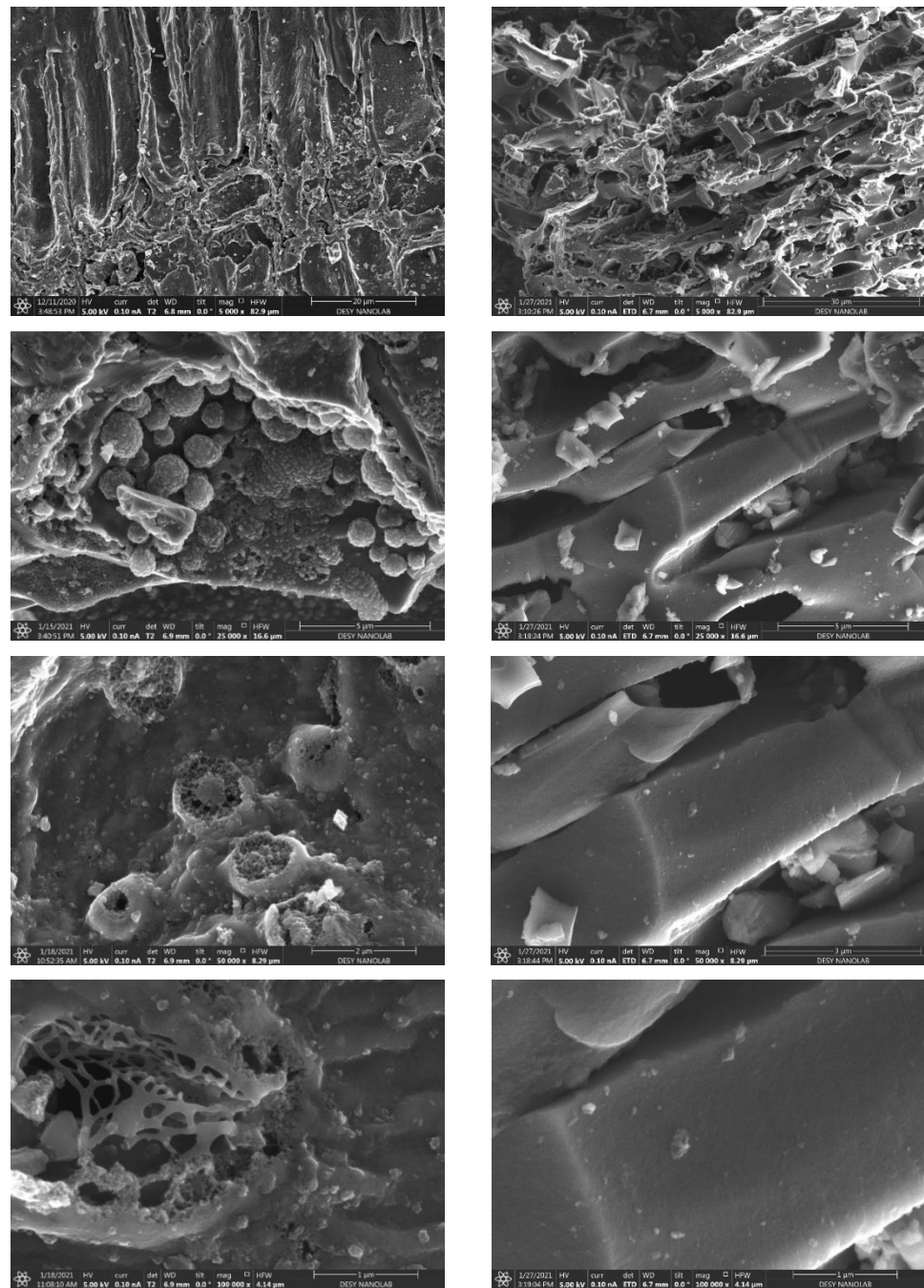


Figure 2. HR-SEM images of the microporous carbons: left set of images—1.18 mm granulation, right set of images—90 μm .

A collection of the XPS scans is shown in Figure 3. A wide scan, Figure 3a, in the region from 100 to 1400 eV, revealed that the carbon and the oxygen were the dominant elements, while some traces of calcium, nitrogen, and chlorine were also revealed. These last three elements were present probably as the remains of the nutrients used by the tree used for the production of carbon and are expected in negligible quantities. More detailed information is needed on the nature of the chemical relations in which carbon and oxygen are involved and, therefore, the XPS narrow spectra of these elements were performed and shown.

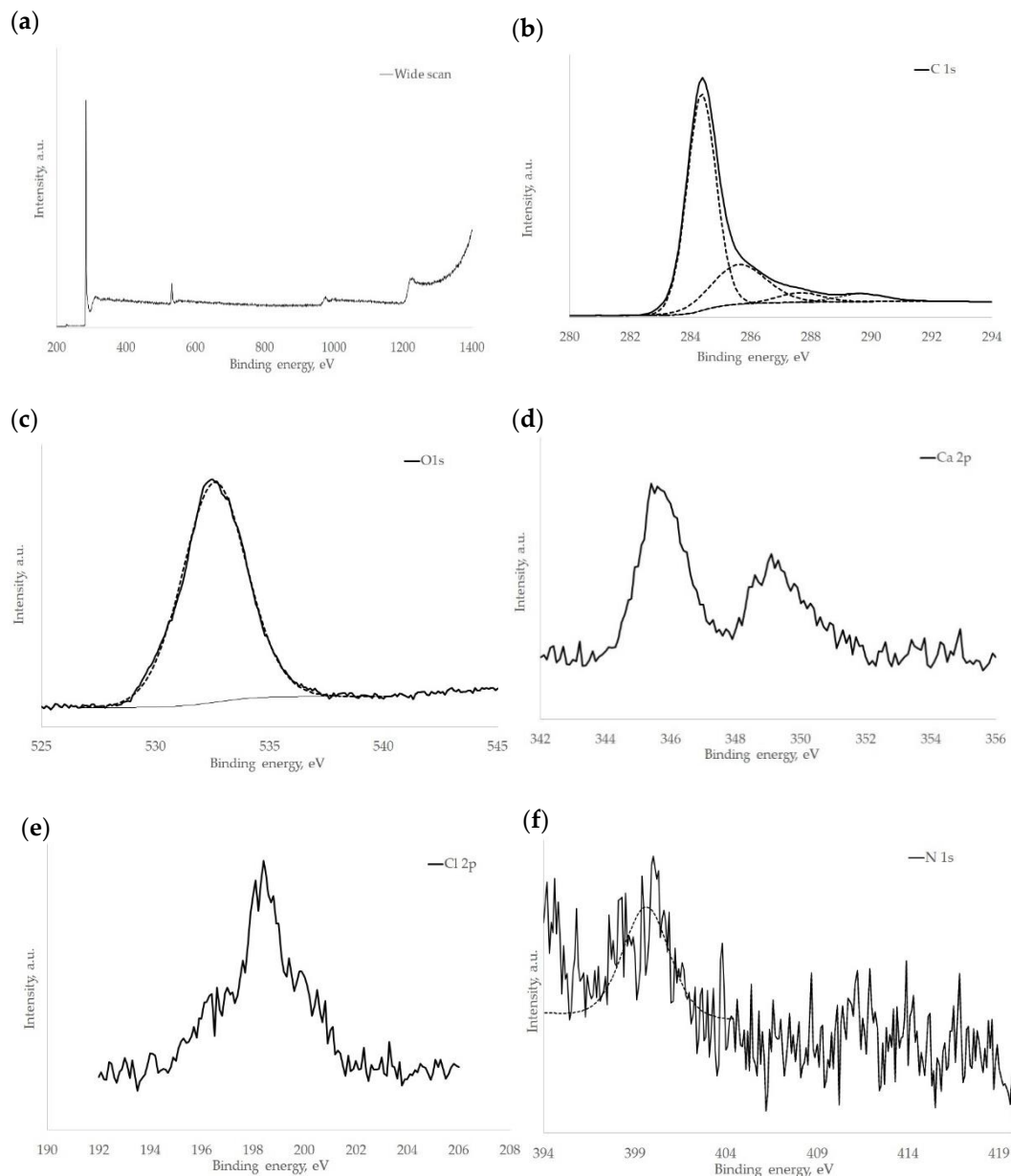


Figure 3. Results of XPS analysis: (a) wide scan, binding energies of: (b) carbon, (c) oxygen, (d) chromium, (e) calcium, (f) nitrogen.

Carbon C1s narrow spectra, Figure 3b, curve fitting showed three prevalent chemical relations in which carbon was involved. These are visible as the peaks shown by dashed lines. The peak at 284.5 eV was expected to be dominant since this binding energy belongs to the graphitic C-C bond and it is clearly visible and in place. The fitted peak at 285.7 eV can belong to the liaison of carbon with S, Cl, or N. Similarly, the fitted peak at 287.7 eV can correspond to the carbon bonded with S, Cl, or N, but can also be a sign of the functional groups forming on the edges of carbon layers, such as alcohols, ethers, and ketones. To resolve this, an O1s narrow spectra (c) was also fitted and it showed only one dominant peak at 532.7 eV. This peak may represent the metal carbonates or the carboxylic group bonding with carbon. Since there was no carboxylic peak visible in the vicinity of 288.5 eV during the carbon 1 s narrow scan (b), it can be concluded that it is probable that the oxygen present represents traces of the calcium carbonate which is naturally present after wood pyrolysis. Calcium as an element is present since the trees are absorbing it as a nutrient from the soil. The presence of the calcium from metal carbonate was confirmed by typical peaks at the Ca 2p scans (d), although some charging occurred in

this narrow scan. Clear presence for chlorine was also confirmed in the narrow scan of Cl 2p electron (e), with the position at 198.5 eV, which corresponds to the metal chlorides. Again, this is probably the nutritive chlorine which was bound to the sodium chloride or other chloride salts absorbed by the tree during its development. However, this presence can be used for the discussion since chloride ions could influence the blasting properties. The narrow spectra of the N 1s (f) was quite difficult to analyze and, due to a lot of noise, it was not very conclusive. It can be said with certainty that the quantity is small and that the peak at 400 eV perfectly corresponds to the C-NH₂ bond which is quite common on the edges of the carbon species produced by pyrolytic methods in general.

An adsorption analysis of the N₂ as well as pore size distribution is presented in Figures 4 and 5. The aim of these analyses was to make preliminary research of the possible influence of these MC-enhancer characteristics on the post-blast oxides generated during the detonation of non-ideal explosives.

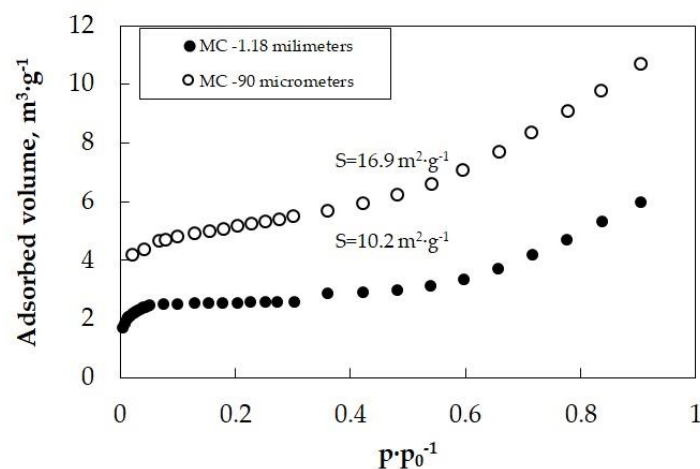


Figure 4. Nitrogen adsorption isotherm of the MC sample.

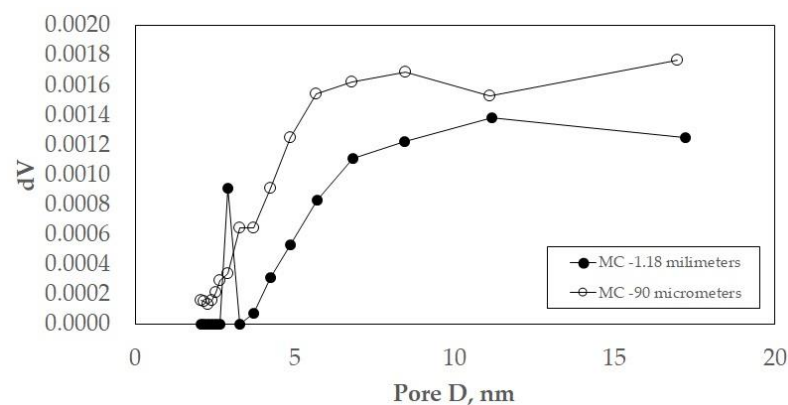


Figure 5. Pore size distribution of the MC sample.

The N₂ adsorption, Figure 4, showed that the specific BET surface of the –1.18 mm granulated charcoal had a lower value of ca. 10.2 m²·g^{−1}. This result is in contrast to the HRSEM images of the present sample (Figure 2, left) and by the similar samples used in a previous study [22] where it was established that some structures of high porosity and complex surfaces are developed and visible. However, based on Figure 5, it was established that the dominant pore size in this sample was 2.9 nm and all of the pores were in the region below 20 nm diameter. Consultations with the experts from the industry revealed that it can be assumed that the actual specific surface is much higher; however, the pores were clogged due to the process itself, i.e., the exhaust gasses were turned back to the furnace in order to prevent the self-incineration of the material during the process of the

pyrolysis. Therefore, it is probable that gas molecules such as SO_x , NO_x , CO_x , as well as some larger molecules which were believed to have evaporated in the process were actually adsorbed and clogged the pores. This should be considered especially during post-blast fume analysis. On the other hand, the carbon of $-90\ \mu\text{m}$ granulation had a somewhat higher specific surface of $16.9\ \text{m}^2\cdot\text{g}^{-1}$. On the contrary, its most dominant pore sizes are 8.4 and 16.9 nm, as can be verified in Figure 6. One explanation can be that the collapse of the structure under intensive milling crushed some of the smallest pores while some new, though larger pores opened along the structure, probably at some harder or even calcified regions (calcium carbonate was confirmed and already verified in the XPS spectra above).

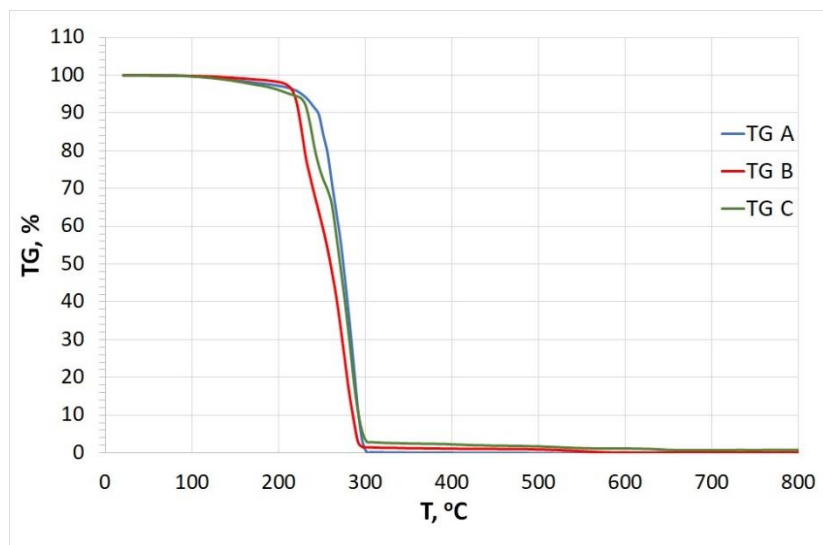


Figure 6. TG results of explosives containing microstructure charcoal grains of $-1.18\ \text{mm}$, sample 2 (TG A), sample 3 (TG B), sample 4 (TG C).

2.4. Explosive's Theoretical Properties

Calculated blasting properties, summarized in Table 2, indicated the potential influence of MC on the tested explosive properties. However, the change of the oxygen balance influences the velocity of detonation in non-ideal explosives (peak VOD when oxygen balance is close to zero and release of the energy is almost complete). Moreover, a decrease of energy with increased content of MC should be followed by the decrease of enthalpy which in the end may affect the explosives sensitivity and critical diameter. In other words, with increased MC content, an explosive material will require higher heat of explosion from the primer, which means that this explosive will be less sensitive than the explosive which was theoretically calculated. Moreover, theoretical calculation indicated that the enthalpy decreases with the addition of MC. However, despite this fact, and by taking into consideration the non-ideal model of the detonation process, the MC should combust behind the reaction front [30]. Under normal conditions, when the inert component which is characterized by the high-standard enthalpy of formation is provided to the explosive composition, an increase in blasting parameters like detonation temperature and pressure takes place. This increase of the detonation temperature will be present until the component which was added to the explosive composition is completely burnt near the Chapman-Jouguet plain. A subsequent change of temperature and pressure (both should decrease) will be accompanied by a drop in the VOD. This effect can be simply explained by the size of the reaction zone. Added MC results with an increase of the active surface. This caused both heat transfer and raised a chemical reaction surface. On the other hand, the addition of MC resulted with a decrease in the induction time of the initiation. Hence, the detonation pressure and temperature both decreased (Table 1). This decrease could be explained by the increase of the surface of the chemical reaction which, in the end, affects both the chemical reaction surface (increases) and the induction time for the initiation (decreases). Moreover,

MC addition will result with the shifting of the oxygen balance towards negative values. This can be explained by the replacement of hydrogen atoms from AN by carbon atoms from fuel oil. In other words, adding MC to the explosive chemical composition results in shifting the oxygen balance toward more negative values which, in the end, may result in additional content of carbon monoxide and soot appearing in gaseous products. These products of the detonation process can make a further impact on the afterburning effect as secondary reactions. The presence of secondary reactions, which are the result of the afterburning, may lead to an increase in the detonation pressure [31]. Salzano and Basco in their afterburning research concluded that black powder afterburning generated a level of the energy which was comparable to the afterburning energy of TNT [31]. The afterburning effect was not included in the ZMWCyw software. Moreover, due to the specific properties of the MC surface, it is expected that the MC content will influence the volume of the CO_x and NO_x in the post-blast fumes, which may hamper the afterburning effect.

Table 2. Theoretical properties of non-ideal explosives.

Parameters	Sample 1	Sample 2	Sample 3	Sample 4
Enthalpy, kJ·kg ⁻¹	−4287	−4269	−4232	−4141
Detonation pressure, MPa	2785	2740	2799	2955
Detonation temperature, K	2701	2675	2593	2458
Heat of explosion, kJ·kg	4012	3922	3695	3588
Strength of the explosion.	976	957	911	911
Post-blast volume, dm ³ ·kg ⁻¹	986	977	959	1013
Density, kg·m ⁻³	821	835	863	864
VOD, m·s ⁻¹	2304	2266	2215	2432
Oxygen balance, %	−1.73	0.83	2.34	−10.34

Moreover, based on the potential blasting properties presented in Table 2, it can be observed that the decrease in detonation temperature and the increase in pressure was generally followed by a drop in the explosion heat, in the post-blast volume, and the strength of the explosive. This influence can be explained by the conversion of mass and momentum equations that represent relationships between the detonation pressure, the velocity of detonation, and the post-blast volume that further affects the Chapman-Jouguet plain [32]. Furthermore, Hugoniot's equations indicate an equilibrium state being independent of the explosive density or the density of the post-blast fumes, confirming the potential drop in the velocity of detonation.

2.5. Explosive's Properties

TG data (Figures 6 and 7) indicated that in all cases, a small mass loss (below 200 °C) was due to the evaporation of FO from the surface of crystalline AN. A further increase in the temperature resulted in a total decrease in the mass of all studied samples, which can be explained by the decomposition of AN according to the following equation [33]:



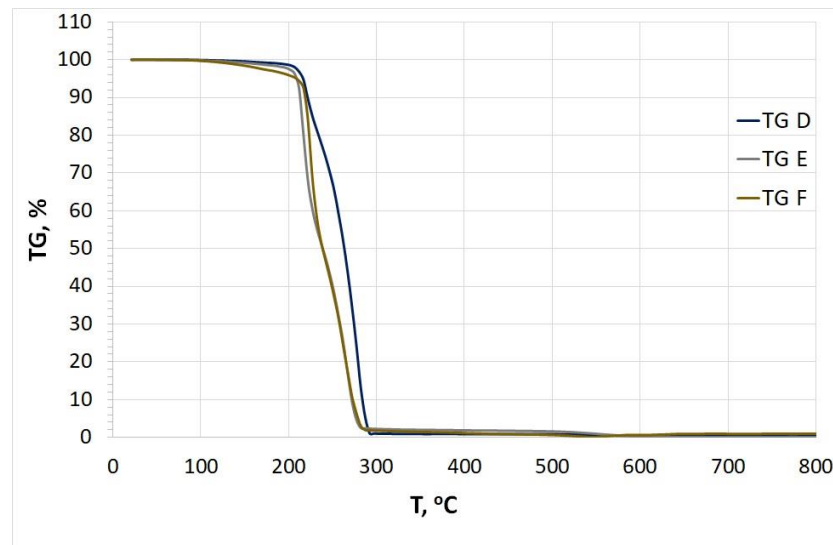


Figure 7. TG results of explosives containing microstructure charcoal grains of $-90\ \mu\text{m}$, sample 2 (TG A), sample 3 (TG B), sample 4 (TG C).

The susceptibility of AN-based explosives to decomposition depended weakly on either the size of MC grains or the chemical composition of the prepared samples. The explosives with lower FO (2.5 wt%) and containing a higher amount of MC (3 wt%) underwent decomposition in the first place. In turn, the samples containing 1 wt% of MC and 4.5 wt% of FO seemed to be most thermally stable.

Figures 8 and 9 illustrate DSC curves at 20–800 °C, obtained for the AN-based explosives containing both FO and MC. In all cases, the DSC profiles indicated four endothermic peaks at 61, 136, 176, and 272–292 °C. Two peaks at ca. 61 and ca. 136 °C were due to the crystallographic transformation of AN III→II and AN II→I, respectively. A third signal at ca. 176 °C originated from the melting point of the AN [24].

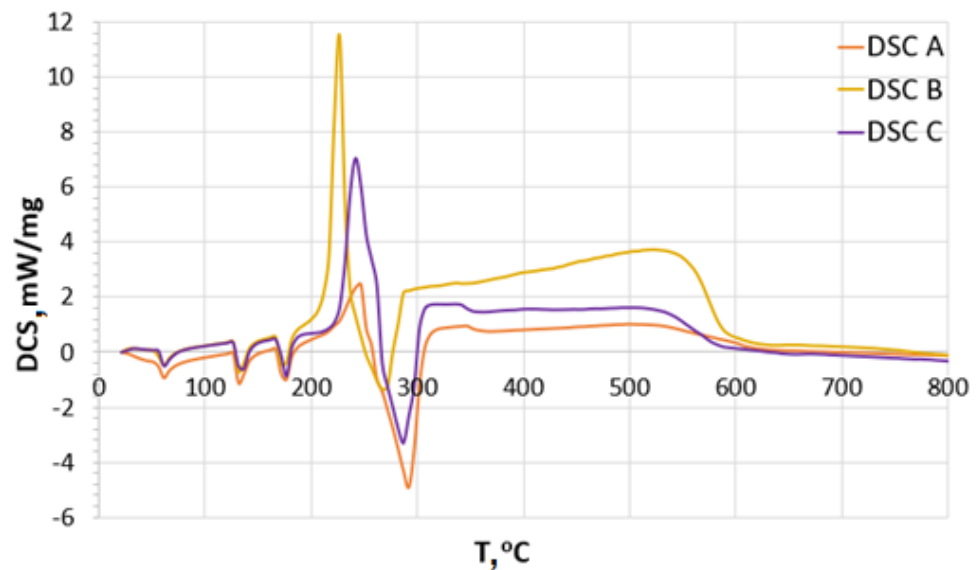


Figure 8. DSC results of explosives containing microstructure charcoal grains of 1.18 mm, sample 2 (TG A), sample 3 (TG B), sample 4 (TG C).

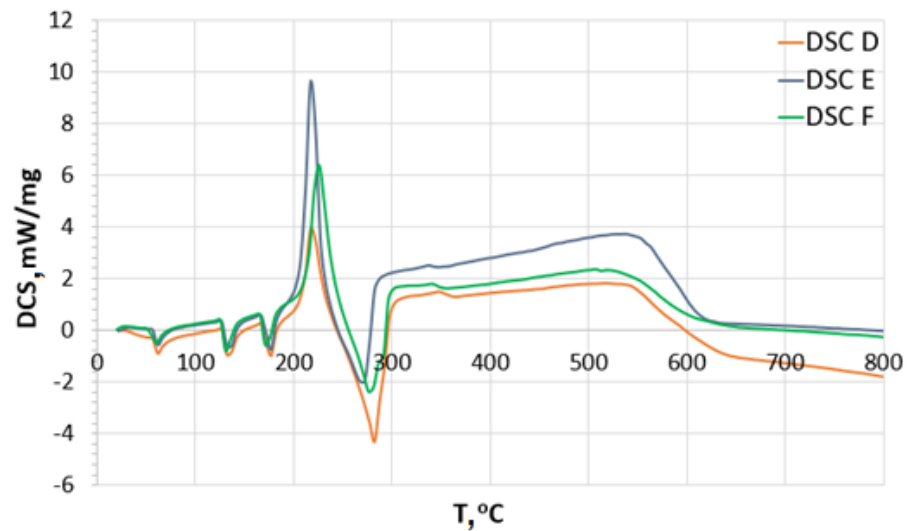


Figure 9. DSC results of explosives containing microstructure charcoal grains of 90 μm , sample 2 (TG A), sample 3 (TG B), sample 4 (TG C).

The increase in temperature led to thermal decomposition of AN, for which the temperature of the fourth DSC peak depended on both the size of the MC grains and the chemical composition of the prepared samples. It was shown that the lowest temperature of decomposition of the investigated explosives was found for the samples containing 2.5 wt% of FO and 3% wt% of MC (272 °C for both samples containing MC grains of -1.18 mm and $-90\ \mu\text{m}$). The highest temperature of the decomposition of the studied materials was found for the samples containing 4.5 wt% of FO and 1 wt% of MC (292 °C and 282 °C for the samples modified with microstructure charcoal grains of -1.18 mm and $-90\ \mu\text{m}$, respectively).

Furthermore, it may be concluded from the obtained data that the size of MC influenced the decomposition reaction. For the samples containing MC, grains of -1.18 mm , DSC endothermic peaks occurred at 272–292 °C, while for counterparts modified with smaller MC particles of $-90\ \mu\text{m}$, the DSC peaks were found at 272–282 °C. This shows that smaller MC grains enable the decomposition of materials prepared in such a way. The DCS data correlates with the TG profiles.

Results of blasting tests of non-ideal explosives where -1.18 mm and $-90\ \mu\text{m}$ MC powders were used are presented in Tables 3 and 4. The obtained results verified some explosive properties which were established based on the thermodynamic models, Table 2.

Table 3. In-situ properties of non-ideal explosives with a microstructure charcoal enhancer of -1.18 mm grain.

Average Parameters	Sample 1	Sample 2	Sample 3	Sample 4
Density, $\text{kg}\cdot\text{m}^{-3}$	800	717	695	722
VOD, $\text{m}\cdot\text{s}^{-1}$	1586	1821	1617	1788
Volume of CO_2 , $\text{dm}^3\cdot\text{kg}^{-1}$	94.19	96.98	109.54	116.05
Volume of CO, $\text{dm}^3\cdot\text{kg}^{-1}$	13.91	9.01	4.65	36.15
Volume of NO, $\text{dm}^3\cdot\text{kg}^{-1}$	1.53	3.84	11.79	7.89
Volume of NO_2 , $\text{dm}^3\cdot\text{kg}^{-1}$	0.11	0.20	0.84	0.45
Volume of NO_x , $\text{dm}^3\cdot\text{kg}^{-1}$	1.64	4.05	12.62	8.34
Total Volume of CO_x and NO_x post-blast fumes, $\text{dm}^3\cdot\text{kg}^{-1}$	109.74	110.04	126.81	160.54

Table 4. In-situ properties of non-ideal explosives with a microstructure charcoal enhancer of $-90 \mu\text{m}$ grain.

Average Parameters	Sample 1	Sample 2	Sample 3	Sample 4
Density, $\text{kg}\cdot\text{m}^{-3}$	800	720	706	726
VOD, $\text{m}\cdot\text{s}^{-1}$	1586	2046	1820	2010
Volume of CO_2 , $\text{dm}^3\cdot\text{kg}^{-1}$	94.19	100.96	111.57	127.43
Volume of CO $\text{dm}^3\cdot\text{kg}^{-1}$	13.91	8.51	2.83	32.80
Volume of NO , $\text{dm}^3\cdot\text{kg}^{-1}$	1.53	5.07	10.63	10.65
Volume of NO_2 , $\text{dm}^3\cdot\text{kg}^{-1}$	0.11	0.23	05.52	0.40
Volume of NO_x , $\text{dm}^3\cdot\text{kg}^{-1}$	1.64	5.30	11.15	11.05
Total Volume of CO_x and NO_x post-blast fumes, $\text{dm}^3\cdot\text{kg}^{-1}$	109.74	114.77	125.55	171.28

Obtained VOD values, Tables 3 and 4, indicated the non-ideal character of tested explosives and confirms the research in [9,13]. Depending on the microstructure grain size, measured VODs were in the range of $1500\text{--}2050 \text{ m}\cdot\text{s}^{-1}$. The measured velocities were lower than predicted from the theoretical calculation (in the range of ca. $2200\text{--}2400 \text{ m}\cdot\text{s}^{-1}$). This derived from the properties of the non-ideal explosives (a decrease of explosive density plays a major role due to the explosive density-VOD relation). Regardless of the grain size, it was observed that MC addition resulted in an increase of the CO_2 content (in the case of MC addition of the grain size of -1.18 mm an increase volume of CO_x and NO_x from ca. of $94 \text{ dm}^3\cdot\text{kg}^{-1}$ to $116 \text{ dm}^3\cdot\text{kg}^{-1}$, in the case of MC addition of the grain size of $-90 \mu\text{m}$ an increase volume of CO_x and NO_x from ca. of $94 \text{ dm}^3\cdot\text{kg}^{-1}$ to $127 \text{ dm}^3\cdot\text{kg}^{-1}$), and a decrease in CO content (except sample 4) in post-blast, Tables 3 and 4. This change was followed by an increase in the volume of NO_x in post-blast fumes (except sample 4), Tables 3 and 4. This relationship is likely explained by the shifting oxygen balance toward positive values (in the case of samples 1–3), as well as composition change. In the case of samples 1–3, the addition of the MC was followed with a decrease in the fuel component (the total wt. of fuel component is always 6.0% of total non-explosive wt.). This shift can be explained by the presence of oxygen in the microstructure charcoal chemical compositions. This was confirmed by the results of XPS analysis, Figure 3c. Moreover, Muzyka and Topolnicka, as well as Radovic, indicated that the total oxygen content in hard coals is influenced by the degree of the metamorphism [34,35]. In other words, oxygen content decreases with the rank of coal. In the case of hard ranks (flame coal, coking coal, and anthracites), the oxygen content was in the range from 17% up to 2%. In brown coals, the oxygen content can vary between 15–35%. Due to this additional content of oxygen, as well as the fact that the individual share of the fuel component has lower negative oxygen balance in comparison with diesel fuel oil, it can be assumed that the oxygen balance of the explosive composition will have a higher positive oxygen balance than presented in Table 2. This additional oxygen, based on Kistiakowski-Wilson's work, will allow oxidation of CO to CO_2 , which causes an increase in the carbon dioxide content and a decrease in the carbon monoxide content. However, higher oxygen balance results in an increase of the NO_x content. In the case of sample 4, the addition of MC was followed by a decrease in the AN-PP. The additional content of oxygen in MC was not equal to the content which was present in AN-PP. This resulted in obtaining a more negative oxygen balance than calculated (-10.34%), as shown in Table 4. As a result, this will increase the CO_2 volume due to the higher carbon content in the non-ideal explosive chemical composition, as well as an increased volume of CO as the result of oxide deficient and the non-complete oxidation process. The decrease in the grain size influenced both the VOD and total-post-blast volume. It was observed that with a decrease in MC content, the post-blast volume and VOD increased; this can be explained by the detonation mechanism. Added MC reacts outside the shockwave front, which increases both the chemical

reaction zone and heat exchange. This results from Hugoniot's equation with an influence on pressure and volume and in shifting the Chapman-Jouguet point.

In addition to the post-volume, the afterburning effect was included in the analysis, Figures 10 and 11, and Tables 5 and 6.

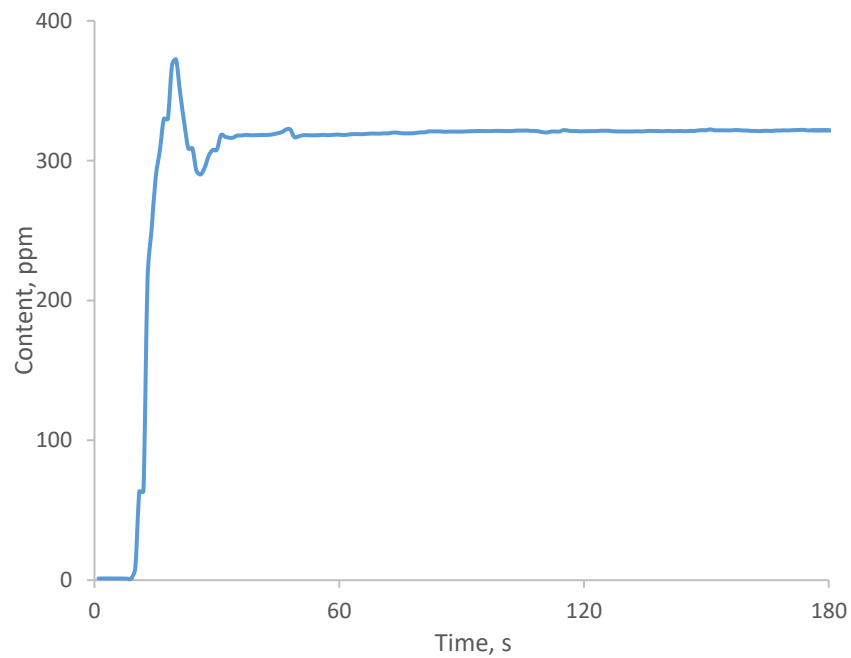


Figure 10. Change of CO content, sample 2, MC of -1.13 mm.

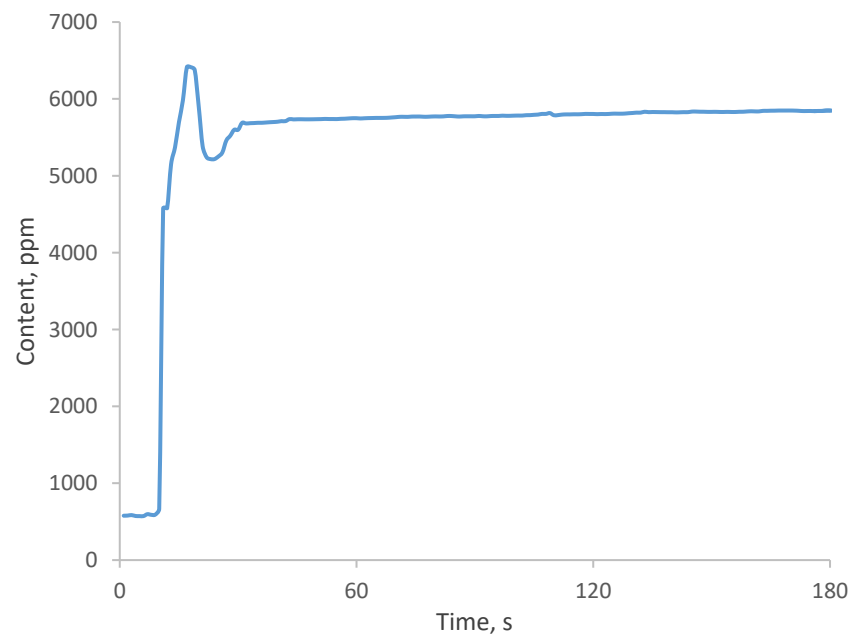


Figure 11. Change of CO₂ content, sample 2, MC of -1.13 mm.

Table 5. Post blast volume of NO_x after 10 min from the detonation microstructure charcoal enhancer of −1.18 mm grain.

Average Parameter	Sample 1	Sample 2	Sample 3	Sample 4
Volume of NO, dm ³ ·kg ^{−1}	1.85	2.42	2.69	3.21
Volume of NO ₂ , dm ³ ·kg ^{−1}	0.18	0.29	0.37	0.72
Volume of NO _x , dm ³ ·kg ^{−1}	2.03	2.71	3.06	3.94

Table 6. Post-blast volume after 10 min, afterburning effect of the non-ideal explosive with a microstructure charcoal enhancer of −90 μm grain.

Average Parameter	Sample 1	Sample 2	Sample 3	Sample 4
Volume of NO, dm ³ ·kg ^{−1}	1.85	2.76	3.56	2.73
Volume of NO ₂ , dm ³ ·kg ^{−1}	0.18	0.46	1.05	0.51
Volume of NO _x , dm ³ ·kg ^{−1}	2.03	3.22	4.62	3.25

The afterburning effect is a result of the secondary reaction between unreacted FO or partially oxidized post-blast fumes which were derived from the primary reactions with the surrounding air. Based on the exemplary record of CO_x, shown in Figures 10 and 11, it can be observed that afterburning appeared in the first minute after the detonation reaction. The first peak of CO (ca. of 370 ppm) and CO₂ (ca. of 6700 ppm) appears to be the direct effect of detonation. Subsequently, afterburning and homogenization appeared, which resulted in the stable volume of the oxides. With a decrease in the oxygen balance, the content of CO will increase (sample 4). The change of the MC diameter did not affect the characteristic of the CO_x volume. It only affected the content of CO_x, and thus the presented records can be treated as model ones. When shifting the oxygen balance toward positive values (sample 2 and sample 3), the content of CO₂ in the primary reaction increased due to the presence of additional oxygen. The products of the decomposition reaction should further influence the afterburning, which results in an increase in the detonation pressure and a shift in the Chapman-Jouguet plain [27]. Moreover, the change of the oxygen balance the secondary reaction which appears from the NO_x should be included (Tables 5 and 6, and Figure 12).

The general record of the NO_x, Figure 12, shows that the first peak is derived from a detonation reaction. The subsequent decrease of NO_x is a result of both homogenization and the decomposition reaction. The small amount of nitrous acid may be an effect of the secondary reaction. However, in contrast to CO_x, it can be observed that the stabilization of the NO_x content takes much longer. Tables 5 and 6 indicate the concentration of NO_x after 10 min from the detonation. The post-blast analysis indicated that oxygen balance affects the content of each individual oxide. In general, based on Tables 3–6, it can be observed that the general ratio between NO/NO_x and NO₂/NO_x decreased with time and stabilized, which suggests the occurrence of secondary reactions and homogenization of the atmosphere in the blasting chamber.

The influence of the MC addition as well as MC grain diameter on the heat of the explosion is presented in Table 7.

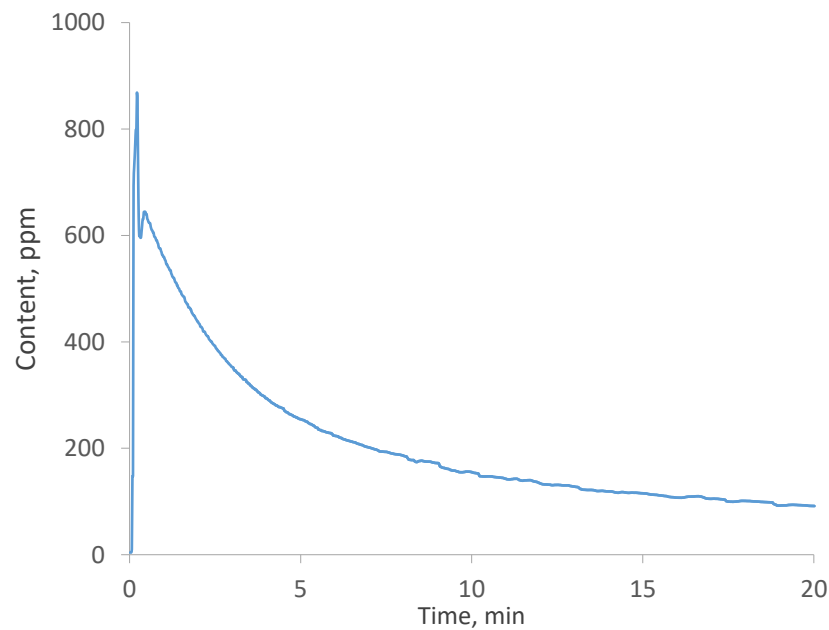


Figure 12. Change of NO_x content, sample 2, MC of -1.13 mm.

Table 7. The heat of the explosion of non-ideal explosives.

Sample	MC Grain Size, mm	Average Energy of Explosion, J·g ⁻¹	Maximum Deflection, %
Sample 1	-	3940	0.5
Sample 2	-0.9	4100	0.3
Sample 3	-0.9	4140	0.2
Sample 2	-1.13	4050	0.2
Sample 3	-1.13	4130	0.1

Based on Table 7, it can be concluded that MC addition slightly increased the average heat of the explosion from $3940 \text{ J}\cdot\text{g}^{-1}$ to within the range of $4050\text{--}4130 \text{ J}\cdot\text{g}^{-1}$ and this depended on the non-explosive composition and grain size. Comparison of the MC grain size led to the conclusion that higher heat explosion values were obtained in the case of non-ideal explosives, where MC powder of the $90 \mu\text{m}$ grain was added. This can be explained by a typical detonation mechanism for the non-ideal explosive with the addition of metal. As stated previously, MC grains undergo a chemical reaction before the shockwave front, which progresses throughout the non-ideal explosive charge. This increases the chemical reaction zone. Moreover, the application of the MC of smaller grain size improves charge density. In the case of explosive charges of higher density, the distance between prills decreases. This has a direct impact on the appearance of hot appearance (smaller gaps between neighboring hot spots), which finally causes lower heat loss [4,36]. In other words, higher charge density improves the chemical reaction zone, the surface of the heat exchange, and reduces heat loss, resulting in an improved detonation temperature and a higher heat of explosion. It can be assumed that the application of the MC powder of smaller grain size could further improve the heat of explosion to a certain point (press point). After reaching the dead-pressed point, the non-ideal explosive should not detonate.

3. Conclusions

In this paper, the influence of MC on blasting properties was investigated. It was established that the use of MC resulted in lower VOD in comparison with values derived from thermodynamic models. This confirmed the non-ideal character of explosives.

Based on the VOD test, it was concluded that a 1.0% addition of MC powder resulted in VOD values of $1821 \text{ m}\cdot\text{s}^{-1}$ and $2046 \text{ m}\cdot\text{s}^{-1}$ and this depended on the size of the MC

grain. By taking into consideration all VOD results, it can be concluded that finer MC powders (90 μm , grains) allowed the highest values of VOD to be obtained. This can be explained by the enhancement of the chemical reaction zone, as well as an increase in heat exchange.

The post-blast oxide analysis showed an elevated volume of CO_2 , NO and NO_2 with an increase in the content of MC powder (sample 2 and sample 3) and a simultaneous decrease of CO volume probably due to an oxygen balance shift towards the positive values. Furthermore, it was found that both VOD and a finer MC powder caused an increase in oxide content. This is evidence of the extension of the chemical reaction zone and the enhancement of heat exchange, which led to the shift of the Chapamn-Jouguet plain.

In the case of sample 4, the influence of oxygen balance which derived mainly from the change of the AN-PP content exhibited the importance of the oxygen balance, especially on post-blast fumes and VOD.

Based on the SEM analysis presented in previous work, it was expected that the NO_x volume should not rise in a near-triple manner. This can be explained not only by the additional oxygen which was present in the MC grain, but also by the low BET surface. It is likely that the areas responsible for the adsorption of nitrous oxides were clogged due to the brittle structure of MC or by its surface (most of its nanopores) already being clogged by the gasses which were evolving during the destructive distillation process. Further tests should be carried out to improve the BET surface, potentially by washing the surface with aromatic and aliphatic solvents. Additionally, the industry could trial processes where the gasses evolved in the destructive process are evacuated instead of remaining in the chamber as they are currently, being used to prevent self-inflammation of the material.

However, based on the obtained data, it can be concluded that the studied type of industrial MC can be applied as an additive to ANFO explosive in the granulations which were the subject of this study. It should be highlighted that the best results were found for the composition of 94.5:4.5:1.0 (AN-PP:FO:MC). It is assumed that further improvements of the MC structure should decrease the volume of NO_x .

Author Contributions: Conceptualization, A.B.; methodology, A.B., S.G.A., M.P. and B.D.N.; validation, A.B., M.P. and M.D.; formal analysis, A.B., S.G.A. and Ł.K.; investigation, S.G.A., A.B., Ł.K., M.D., M.T., M.P., D.N.-S. and B.D.N.; resources, A.B. and S.G.A.; writing—original draft preparation, S.G.A., A.B., Ł.K., M.D., M.T., M.P. and D.N.-S., writing—review and editing, A.B.; visualization, A.B., S.G.A., Ł.K. and M.T.; supervision, A.B. All authors have read and agreed to the published version of the manuscript.

Funding: The authors wish to thank for financial support for research no. 16.16.100.215 of The Faculty of Civil Engineering and Resource Management at the AGH University of Science and Technology in Krakow. HR-SEM and XPS measurements were financed through the NFFA Horizon2020 project (Grant agreement ID: 654360), while the BET equipment was purchased for this study by University of Banja Luka by the national project (Contract number 19.032/961-152/19).

Institutional Review Board Statement: Not applicable.

Informed Consent Statement: Not applicable.

Data Availability Statement: The data presented in this study are available on request from the corresponding author (A.B.).

Conflicts of Interest: The authors wish to confirm that there are no known conflicts of interest associated with this publication and there has been no significant financial support for this work that could have influenced its outcome.

References

1. Maranda, B.; Gołabek, J.; Kasperski, J. *Materiały Wybuchowe Emulsyjne*; Wydawnictwo Naukowo-Techniczne: Warszawa, Poland, 2015.
2. Borowik, M.; Biskupski, A.; Dawidowicz, M.; Buczkowski, D. Rules of Safe Storage of the Ammonium Nitrate Ferlitzers. *Przem. Chem.* **2013**, *92*, 2148–2152.

3. Biessikirski, A.; Kuterasiński, Ł.; Dworzak, M.; Pyra, J.; Twardosz, M. Comparison of structure, morphology, and topography of fertilizer-based explosives applied in the mining industry. *Microchem. J.* **2019**, *144*, 39–44. [[CrossRef](#)]
4. Biessikirski, A. *Research on the Physicochemical Properties of Non-Ideal Explosives Based on Various Types of Ammonium Nitrate(V) and Fuel Oils*; Wydawnictwa AGH: Kraków, Poland, 2020.
5. Landucci, G.; Reniers, G.; Cozzani, V.; Salzano, E. Vulnerability of industrial facilities to attacks with improvised devices aimed at triggering domino scenarios. *Reliab. Eng. Syst. Saf.* **2015**, *143*, 53–62. [[CrossRef](#)]
6. Biessikirski, A.; Kuterasiński, Ł. *Research on Morphology and Topology of ANFO Based on Various Types of Oxygen Component*; Wydawnictwa AGH: Kraków, Poland, 2018; ISBN 978-83-66016-43-9.
7. Zygmunt, B.; Buczkowski, D. Influence of Ammonium Nitrate Prills' Properties on Detonation Velocity of ANFO. *Propellants Explos. Pyrotech.* **2007**, *32*, 411–414. [[CrossRef](#)]
8. Miyake, A.; Takahara, K.; Ogawa, T.; Ogata, Y.; Wada, Y.; Arai, H. Influence of physical properties of ammonium nitrate on the detonation behavior of ANFO. *J. Loss Prev. Process Ind.* **2001**, *14*, 533–538. [[CrossRef](#)]
9. Miyake, A.; Kobayashi, H.; Echigoya, H.; Kubota, S.; Wada, Y.; Ogata, Y.; Arai, H.; Ogawa, T. Detonation characteristics of ammonium nitrate and activated carbon mixtures. *J. Loss Prev. Process Ind.* **2007**, *20*, 584–588. [[CrossRef](#)]
10. Nakamura, H.; Saeki, K.; Akiyoshi, M.; Takahashi, K. The reaction of ammonium nitrate with carbon powder. *J. Jpn. Explos. Soc.* **2002**, *63*, 87–93.
11. Miyake, A.; Echigoya, H.; Kobayashi, H.; Katoh, K.; Kubota, S.; Wada, Y.; Ogata, Y.; Ogawa, T. Detonation velocity and pressure of ammonium nitrate and activated carbon mixtures. *Mater. Sci. Forum* **2008**, *566*, 107–112. [[CrossRef](#)]
12. Miyake, A.; Echigoya, H.; Kobayashi, H.; Ogawa, T.; Katoh, K.; Kubota, S.; Wada, Y.; Ogata, Y. Non-ideal detonation properties of ammonium nitrate and activated carbon mixtures. *Int. J. Mod. Phys. B* **2008**, *22*, 1319–1324. [[CrossRef](#)]
13. Kubota, S.; Saburi, T.; Ogata, Y.; Miyake, A. Non-ideal behaviour of ammonium nitrate based high-energetic materials in small diameter steel tube. *Sci. Technol. Energy Mater.* **2013**, *74*, 61–65.
14. Lurie, B.A.; Lianshen, C. Kinetics and mechanism of thermal decomposition of ammonium nitrate powder under the action of carbon black. *Combust. Explos. Shock Waves* **2000**, *36*, 607–617. [[CrossRef](#)]
15. Izato, Y.-I.; Miyake, A.; Echigoya, H. Influence of the physical properties of carbon on the thermal decomposition behavior of ammonium nitrate and carbon mixtures. *Sci. Technol. Energy Mater.* **2009**, *70*, 101–104.
16. De Souza, E.M.; Katsabanis, P.D. On the prediction of blasting toxic fumes and dilution ventilation. *Min. Sci. Technol.* **1991**, *13*, 223–235. [[CrossRef](#)]
17. Sapko, M.; Rowland, J.; Mainiero, R.; Zlochower, I. Chemical and physical factors that influence NOx production during blasting—exploratory study. In Proceedings of the 28th Conference on 'Explosives and Blasting Technique', Las Vegas, NV, USA, 10 February 2002; pp. 317–330.
18. Mainiero, R.; Harris, M.; Rowland, J. Dangers of toxic fumes from blasting. In Proceedings of the 33rd Conference on 'Explosives and Blasting Technique', Nashville, TN, USA, 28–31 January 2007; Volume 1, pp. 1–6.
19. Onederra, I.; Bailey, V.; Cavanough, G.; Torrance, A. Understanding main causes of nitrogen oxide fumes in surface blasting. *Min. Technol.* **2012**, *121*, 151–159. [[CrossRef](#)]
20. Chaiken, R.F.; Cook, E.B.; Ruhe, T.C. *Toxic Fumes from Explosives: Ammonium Nitrate-Fuel Oil Mixtures*; BuMines RI 7867; US Department of the Interior, Bureau of Mines: Washington, DC, USA, 1974.
21. Rowland, J.H., III; Mainiero, R. Factors Affecting ANFO Fumes Production. In Proceedings of the 26th Annual Conference on Explosives and Blasting Technique, Cleveland, OH, USA, 13–16 February 2000; International Society of Explosives Engineers; pp. 163–174.
22. Atlagic, S.G.; Biessikirski, A.; Kuterasiński, Ł.; Dworzak, M.; Twardosz, M.; Sorogas, N.; Arvanitidis, J. On the Investigation of Microstructured Charcoal as an ANFO Blasting Enhancer. *Energies* **2020**, *13*, 4681. [[CrossRef](#)]
23. Niksiński, A. *Górnictwo Materiały Wybuchowe. Obliczanie Parametrów Użytkowych*; BN-80/6091-42; Zakłady Tworzyw Sztucznych ERG: Bieruń, Poland, 1981.
24. Biessikirski, A.; Pytlik, M.; Kuterasiński, Ł.; Dworzak, M.; Twardosz, M.; Napruszewska, B.D. Influence of the Ammonium Nitrate(V) Porous Prill Assortments and Absorption Index on Ammonium Nitrate Fuel Oil Blasting Properties. *Energies* **2020**, *13*, 3763. [[CrossRef](#)]
25. European Commission. *Explosives for Civil Uses. High Explosives. Part 16: Detection and Measurement of Toxic Gases*; EN 13631-16:2004; European Committee for Standardization: Brussels, Belgium, 2004.
26. European Union. Council directive 93/15/EEC of 5 April 1993 on the harmonization of the provisions relating to the placing on the market and supervision of explosives for civil uses. *Off. J. Eur. Union* **1993**, *12*, 20–36.
27. Zawadzka-Małota, I. Testing of mining explosives with regard to the content of carbon oxides and nitrogen oxides in their detonation products. *J. Sustain. Min.* **2015**, *14*, 173–178. [[CrossRef](#)]
28. European Commission. *Explosives for Civil Uses. High Explosives. Part 14: Determination of Velocity of Detonation*; EN 13631-14:2003; European Committee For Standardization: Brussels, Belgium, 2003.
29. Mertuszka, P.; Pytlik, M. Analysis and comparison of the continuous detonation velocity measurement method with the standard method. *High-Energy Mater.* **2019**, *11*, 63–72.
30. Maranda, A. Influence of aluminium chemical activity on detonation parameters of composite explosives containing aluminium powders (CX-AL). *Wiad. Chem.* **2001**, *55*, 353–375.

31. Salzano, E.; Basco, A. Comparison of the explosion thermodynamics of TNT and black powder using Le Chatelier diagrams. *Propellants Explos. Pyrotech.* **2012**, *37*, 724–731. [[CrossRef](#)]
32. Jackson, S.I. The dependence of Ammonium-Nitrate Fuel-Oil (ANFO) detonation on confinement. *Proc. Combust. Inst.* **2017**, *36*, 2791–2798. [[CrossRef](#)]
33. Babrauskas, V.; Leggett, D. Thermal decomposition of ammonium nitrate. *FAM Fire Mater.* **2020**, *44*, 250–268. [[CrossRef](#)]
34. Muzyk, R.; Topolnicka, T. Direct determination of oxygen content in coals by the use of the high-temperature pyrolysis method. *Prz. Gor.* **2013**, *69*, 100–104.
35. PennState College of Earth and Mineral Sciences. Available online: <https://personal.ems.psu.edu/~radovic/Chapter7.pdf> (accessed on 1 March 2021).
36. Biessikirski, A.; Barański, K.; Pytlik, M.; Kuterasiński, Ł.; Biegańska, J.; Słowiński, K. Application of Silicon Dioxide as the Inert Component or Oxide Component Enhancer in ANFO. *Energies* **2021**, *14*, 2152. [[CrossRef](#)]